Characterization of Lipid A Variants by Energy-Resolved Mass Spectrometry: Impact of Acyl Chains

Christopher M. Crittenden,[1] Lucas D. Akin,[1] Lindsay J. Morrison,[1] M. Stephen Trent,[2] Jennifer S. Brodbelt[1]

[1]Department of Chemistry, University of Texas, Austin, TX 78712
[2]Department of Infectious Diseases, University of Georgia, Athens, Georgia 30602, United States

Supporting Information

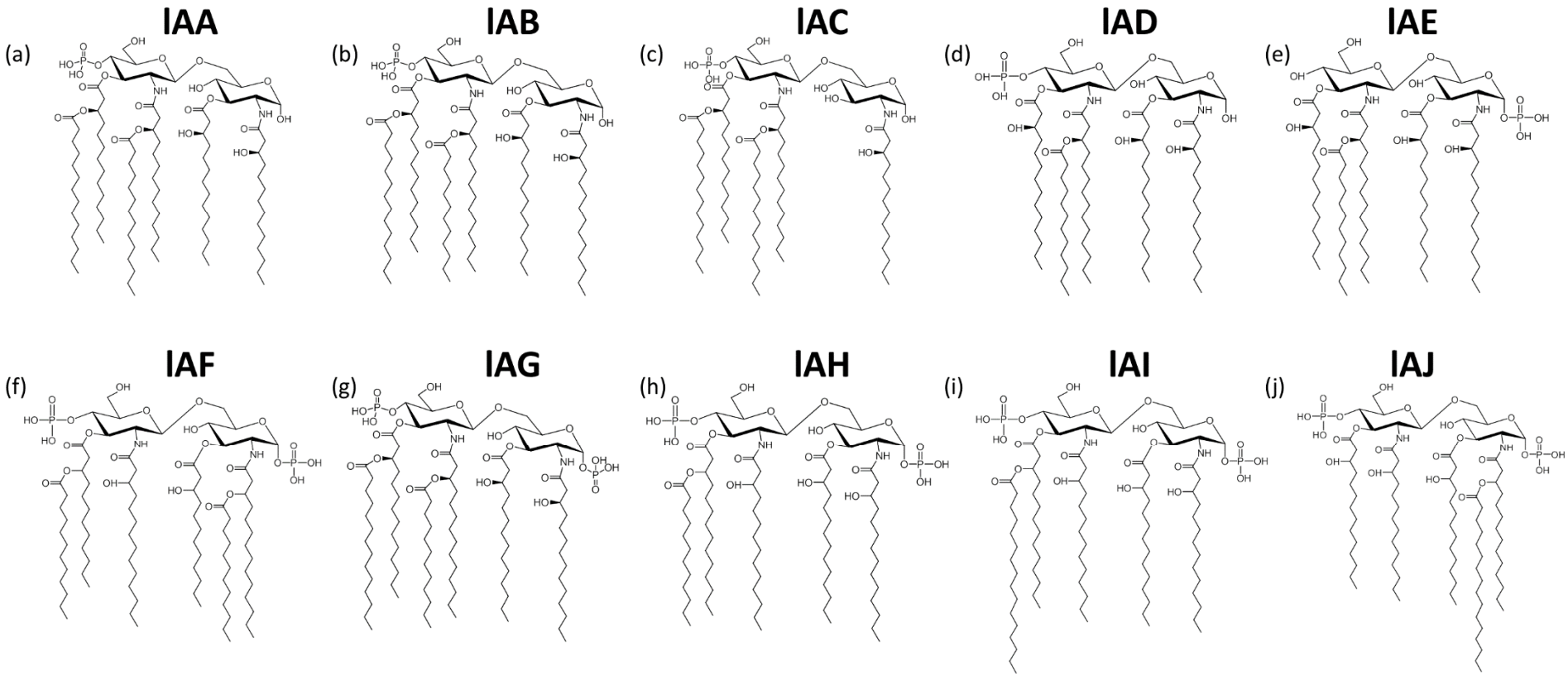

Supplementary Figure S1: All 10 lipid A variants evaluated. (a) monophosphoryl lipid A (1745.28 Da, lAA); (b) detoxified lipid A (1717.25 Da, lAB); (c) monophosphoryl 3-deacyl lipid A (1519.09 Da, lAC); (d) *E. coli* strain BN2E (1507.05 Da, lAD); (e) *E. coli* strain BN2F (1507.05 Da, lAE); (f) *Acinetobacter baumannii* expressing lpxL (1713.13 Da, lAF); (g) bisphosphorylated lipid A (1797.22 Da; lAG); (h) *W. succinogenes* lpxJ (1587.02 Da, lAH); (i) *C. jejuni* 240 0482 (1643.08 Da, lAI); (j) *C. jejuni* lpxJ (1643.08 Da, lAJ)

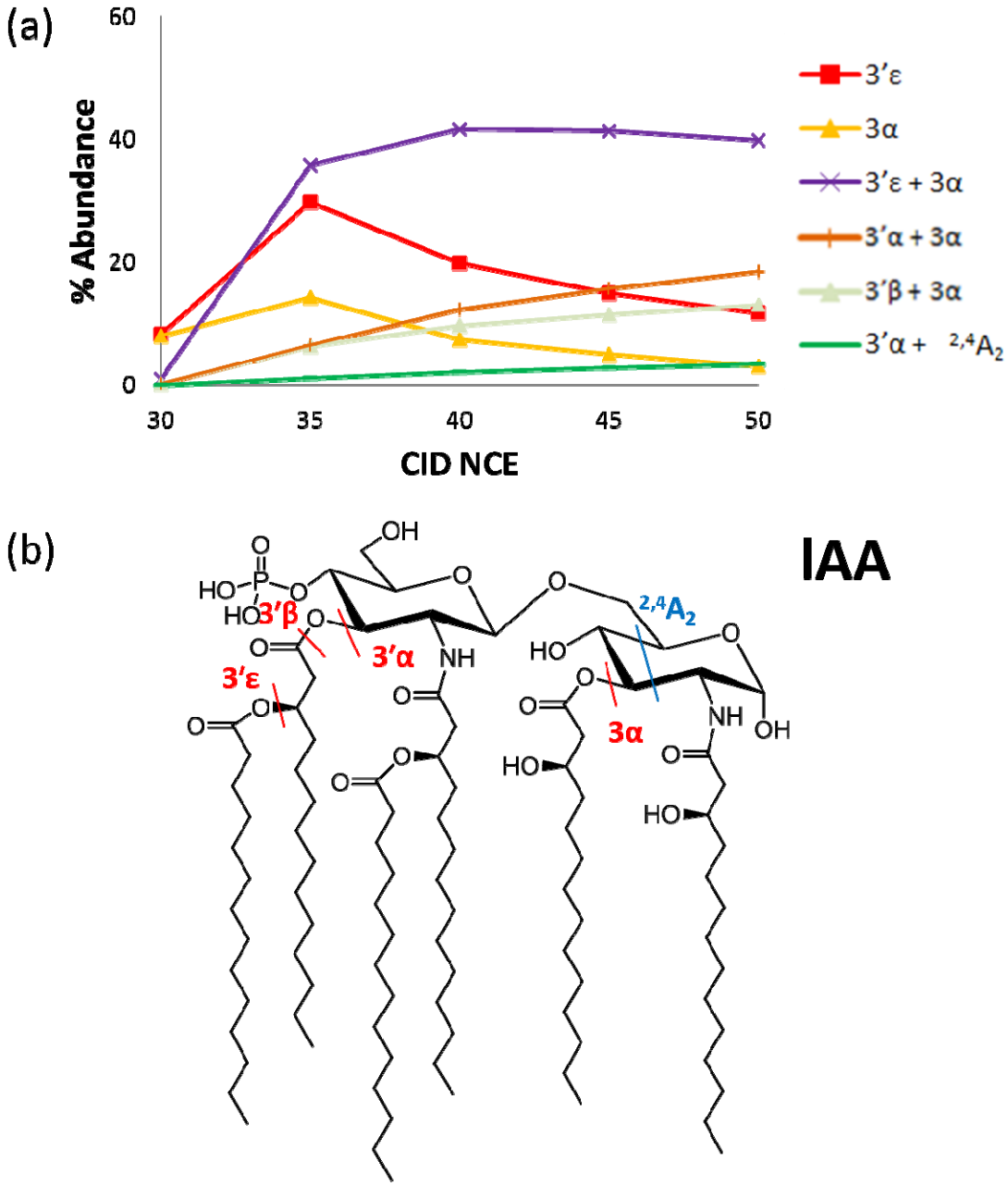

Supplementary Figure S2: (a) CID ERMS of lAA and (b) the structure. CID ERMS does not afford the same genealogical information that HCD and UVPD do.

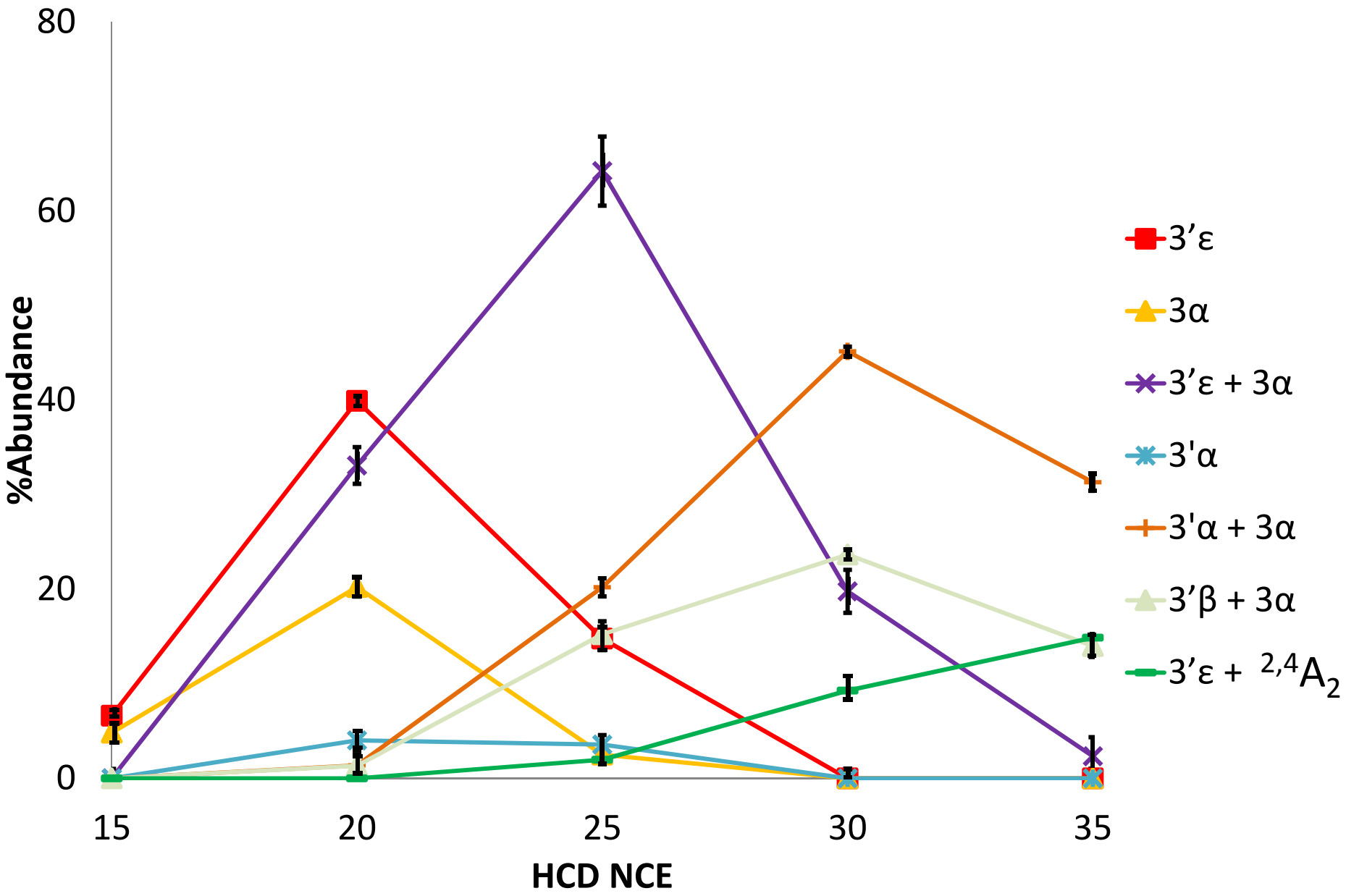

Supplementary Figure S3: HCD ERMS plot of lAA with error bars illustrating the standard deviations of the measurements performed in triplicate.

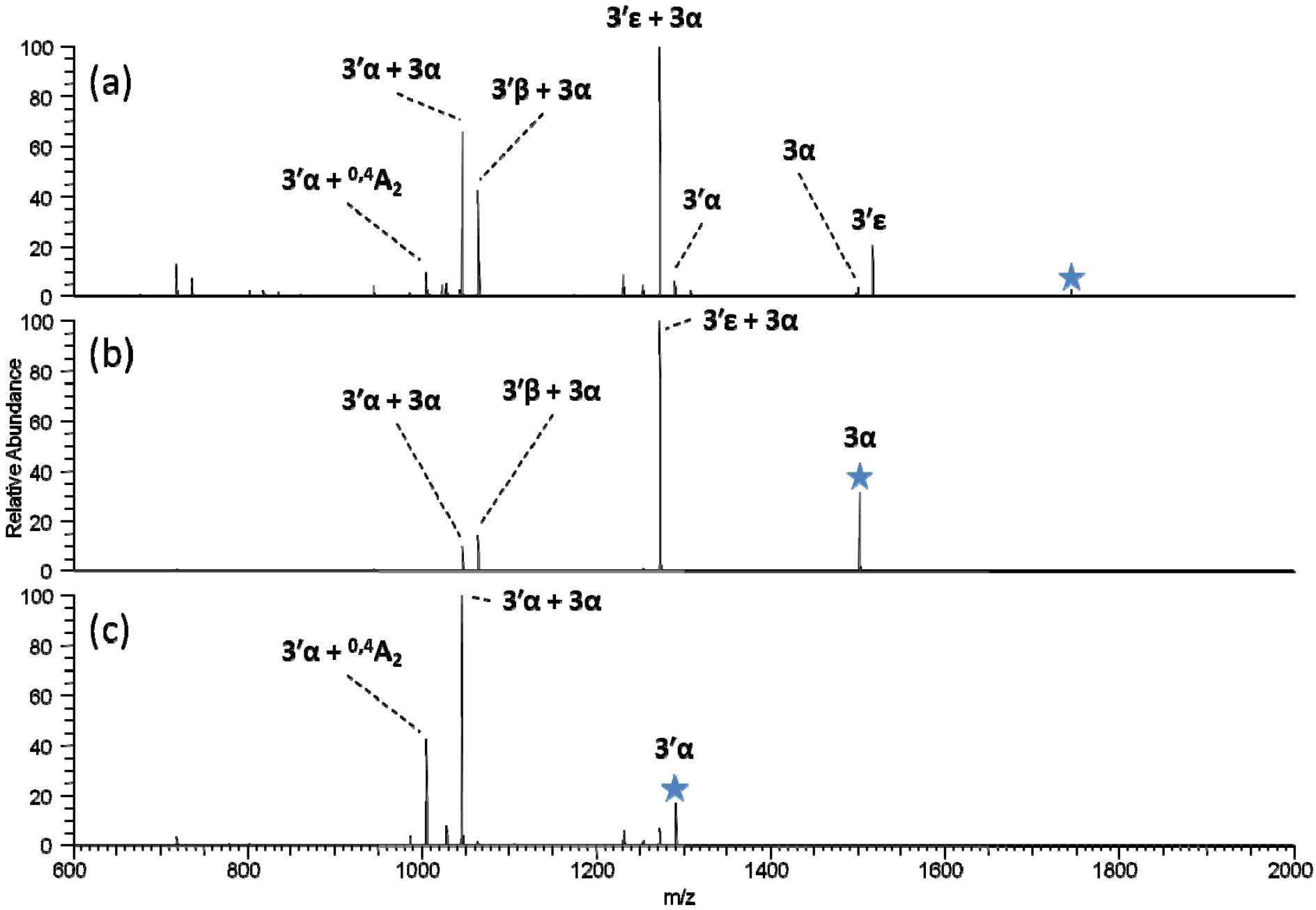

Supplementary Figure S4: (a) MS2 (HCD) on the 1- charge state of lAA. (b) MS3 (HCD) on the 3α peak reveals the procedural loss of the 3'ε, 3'β, and 3'α, respectively. (c) MS3 (HCD) on the 3'α peak reveals loss of 3α and cross-ring cleavage at $^{0,4}A_2$.

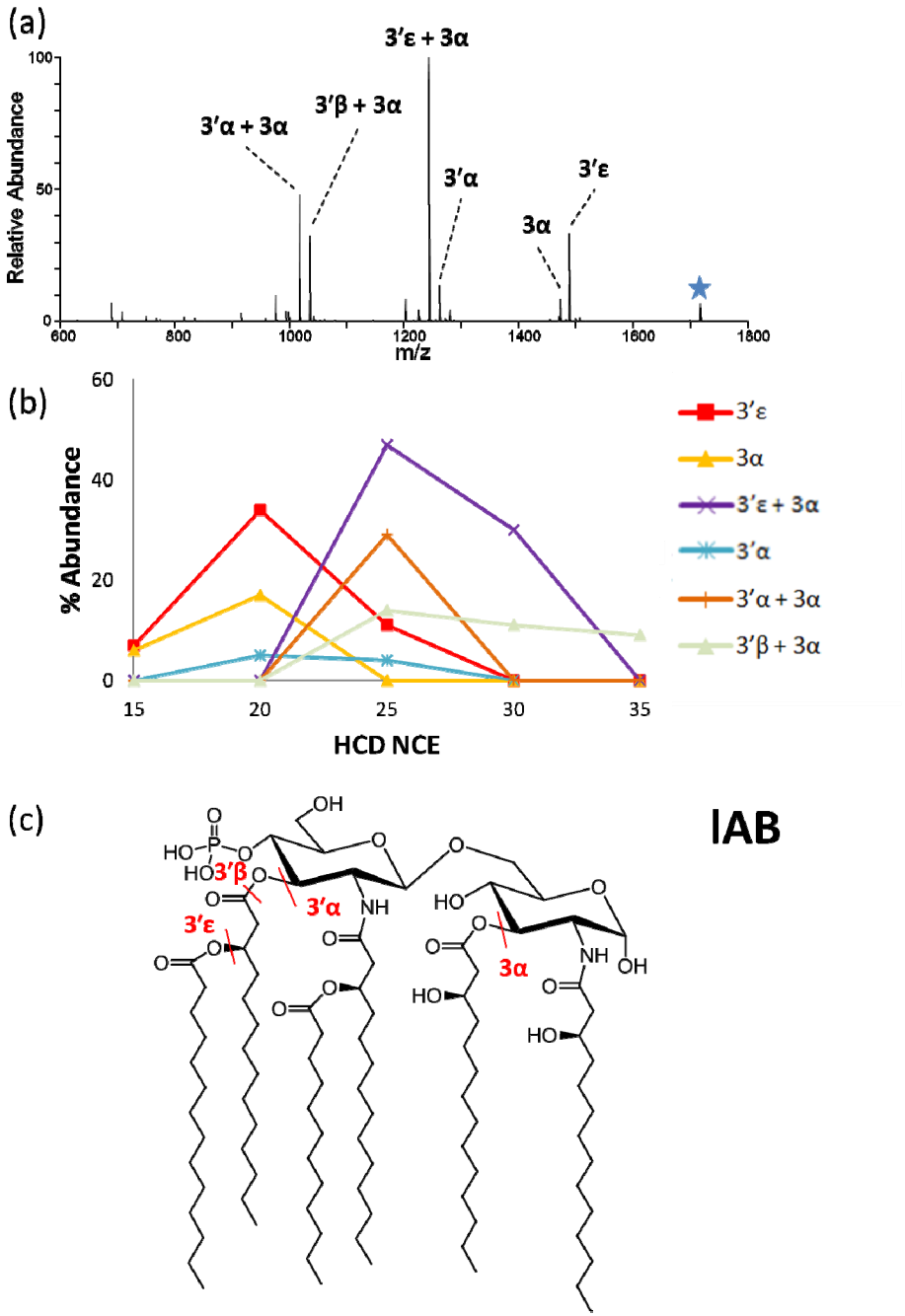

Supplementary Figure S5: lAB MS2 spectra using HCD at NCE=25 (a) and the corresponding HCD ERMS plot (b). The structure of lAB is shown in (c).

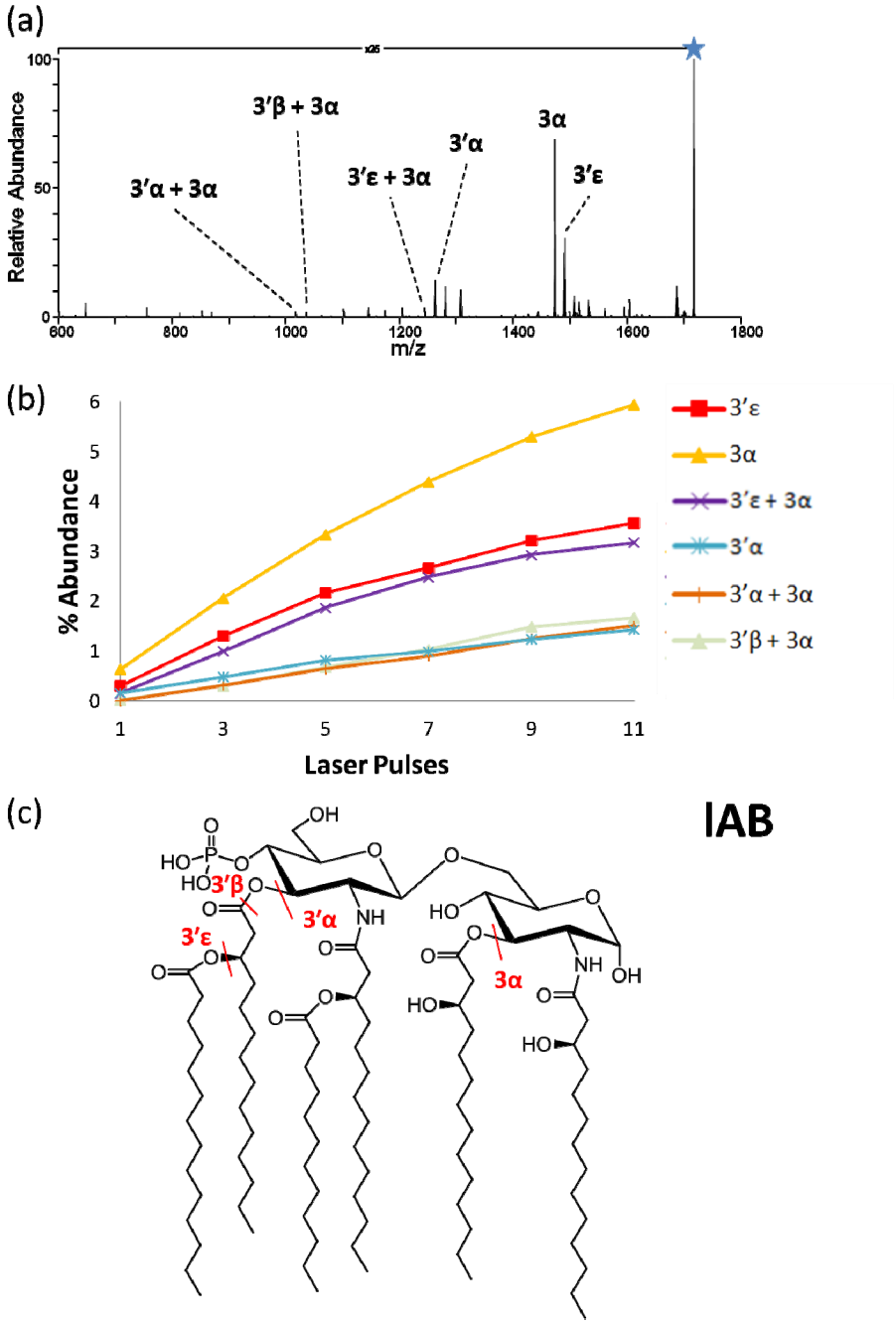

Supplementary Figure S6: lAB MS2 spectra using UVPD at 3mJ, 5 pulses (a) and the corresponding UVPD ERMS plot (b). The structure for lAB is shown in (c).

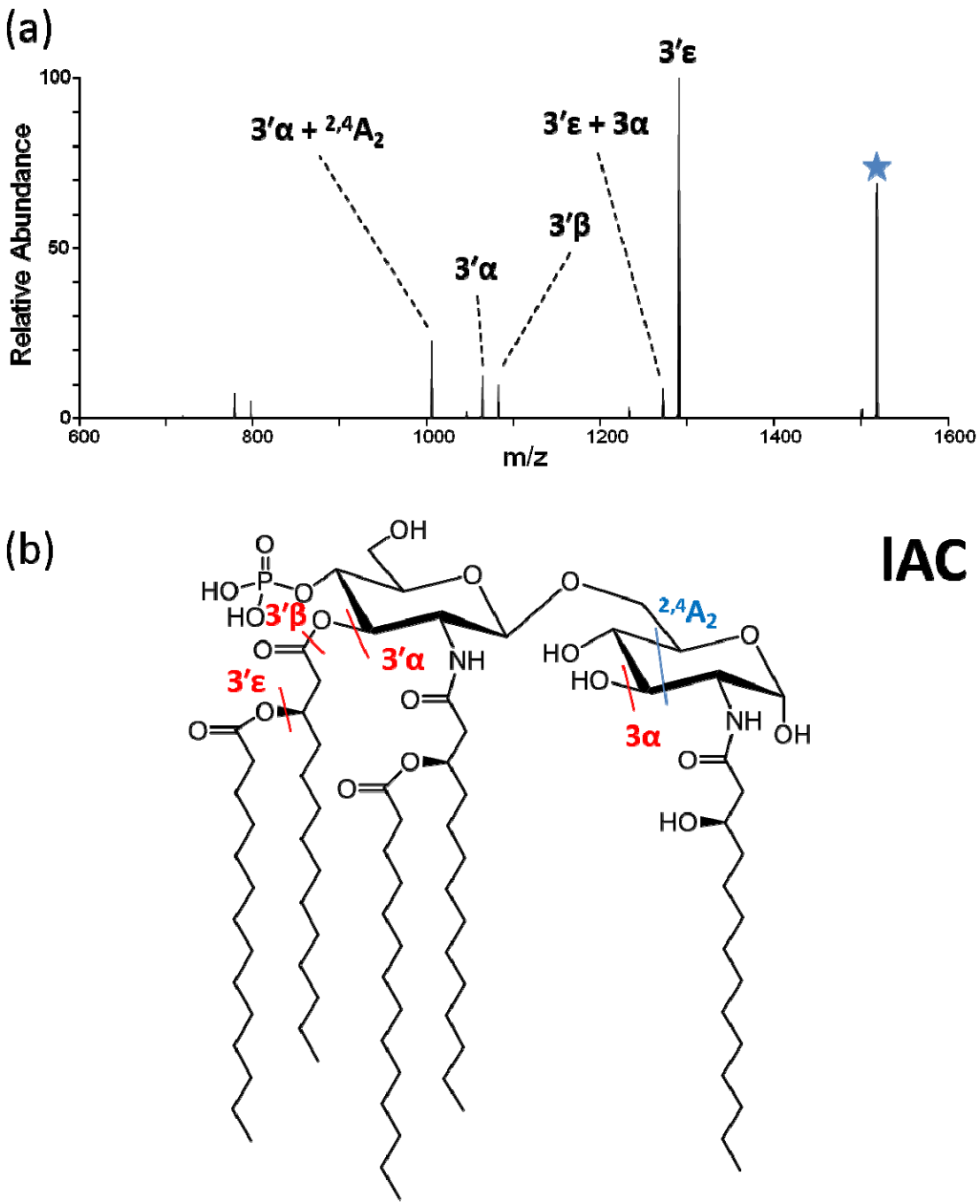

Supplementary Figure S7: MS2 HCD spectra of lAC at NCE=20. The structure of lAC is shown in (b).

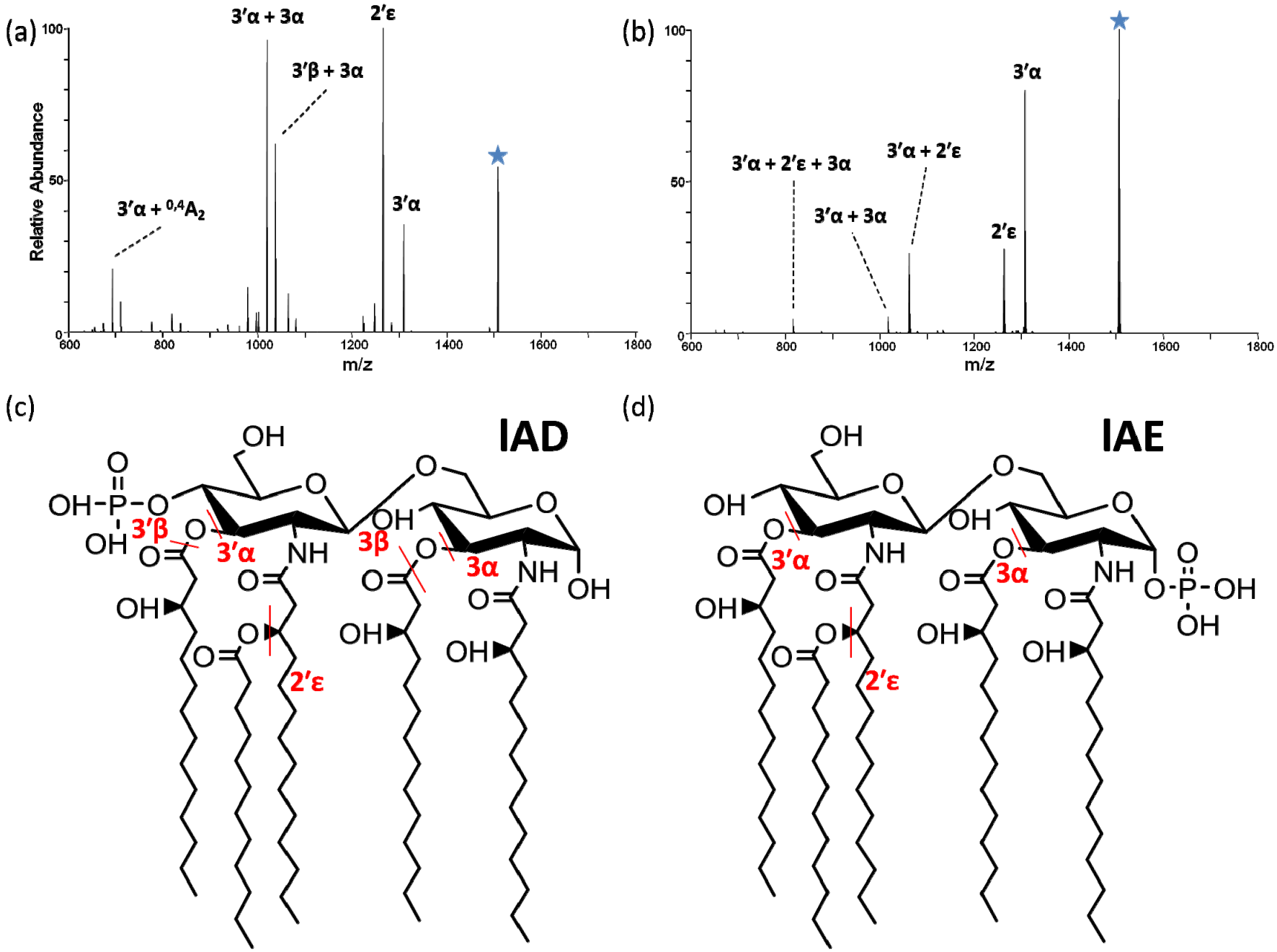

Supplementary Figure S8: MS2 HCD spectra of (a) lAD and (b) lAE at NCE=25 and their structures (c) and (d), respectively.

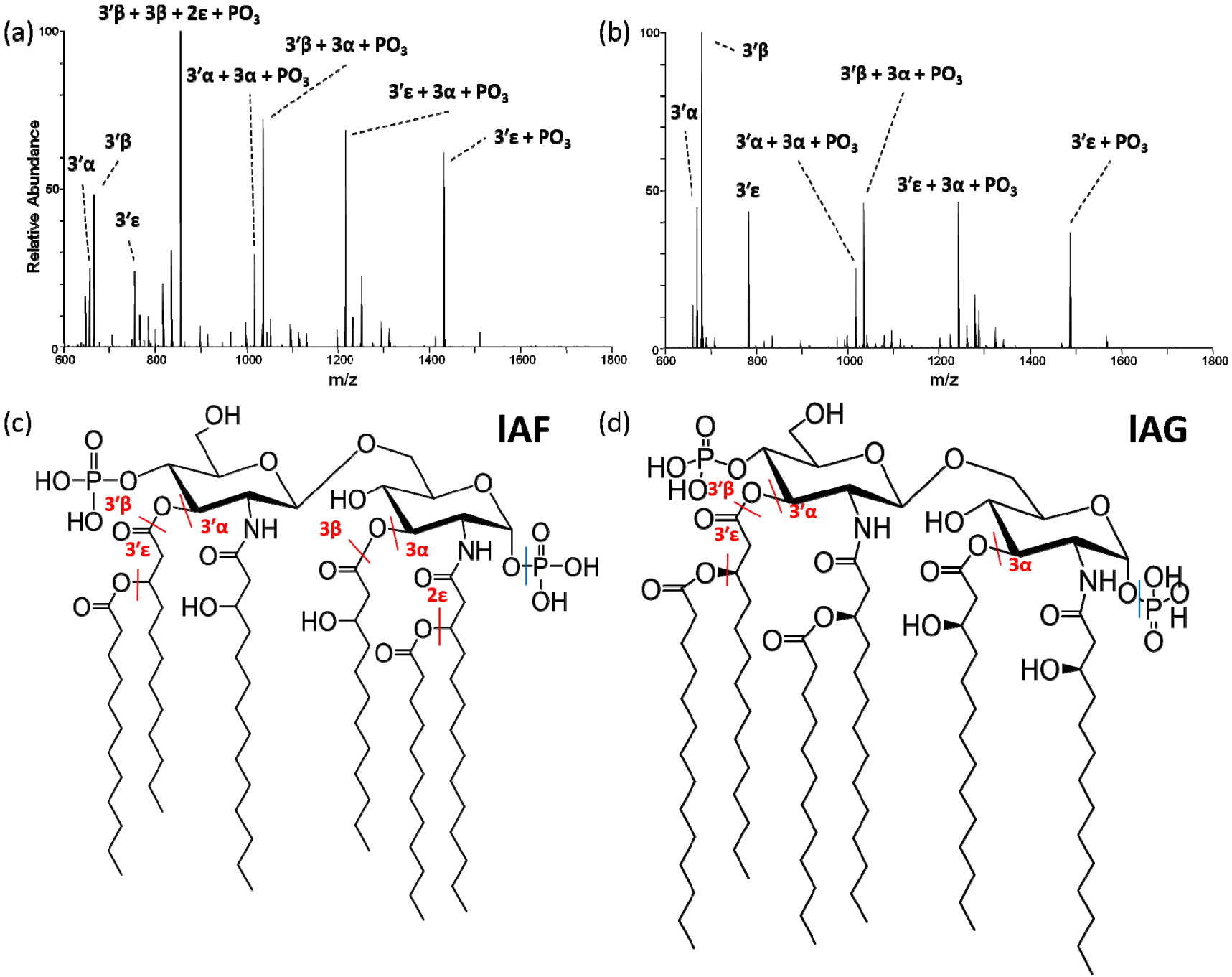

Supplementary Figure S9: MS2 HCD spectra of (a) lAF and (b) lAG at NCE=30 and their structures (c) and (d), respectively.

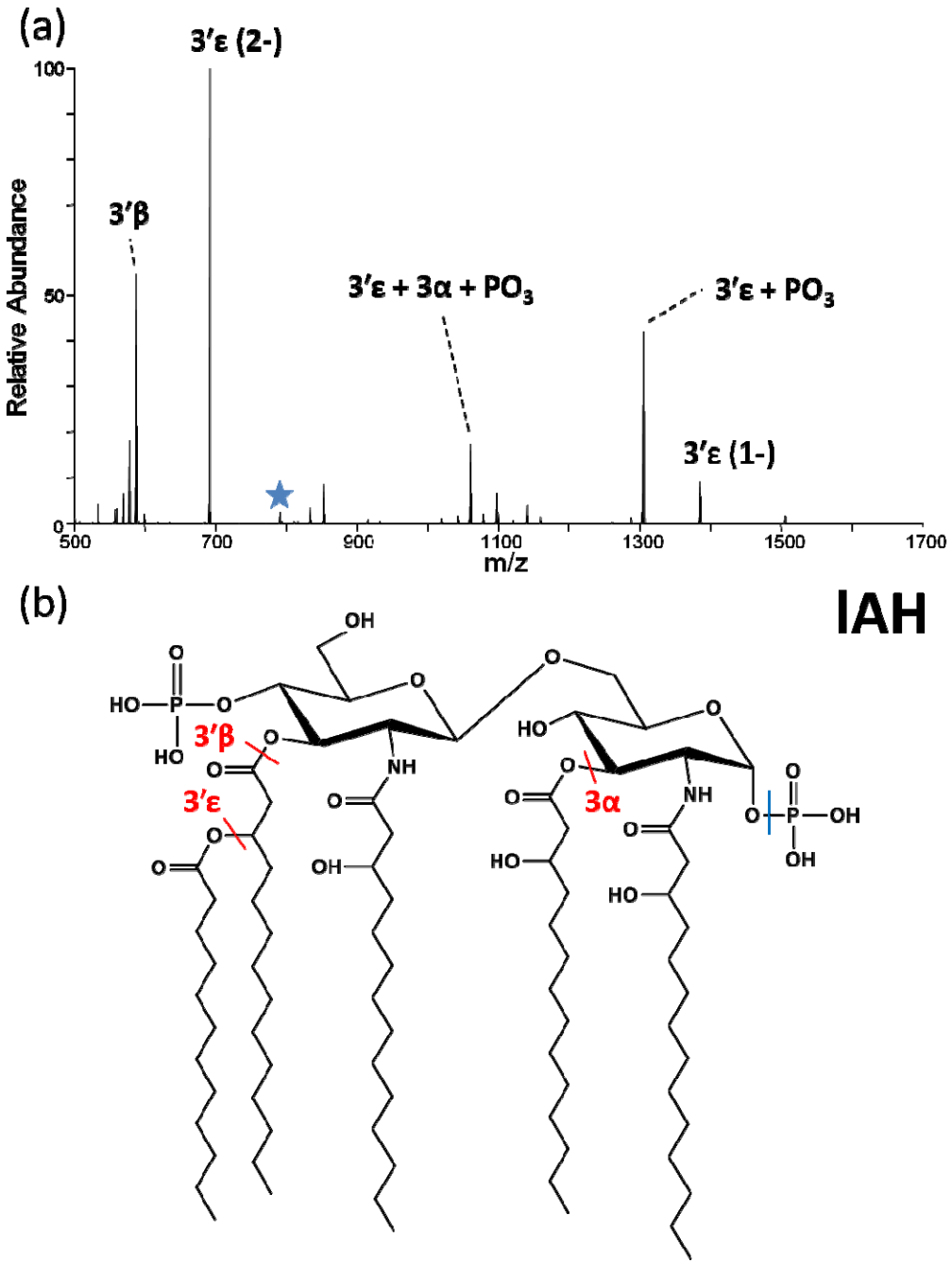

Supplementary Figure S10: lAH MS2 spectra using HCD at NCE=25 (a). The structure of lAH is shown in (b).

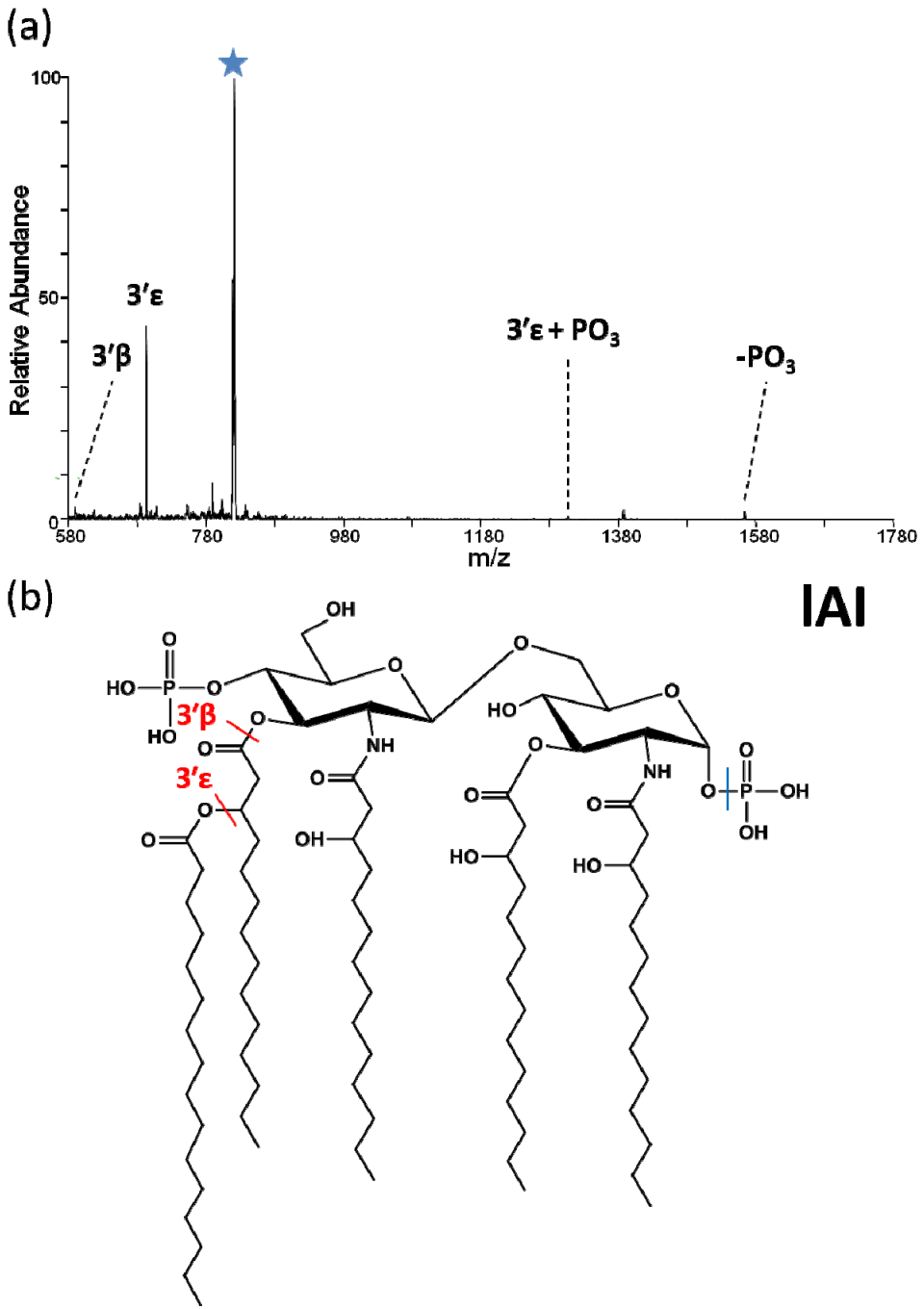

Supplementary Figure S11: lAI MS2 spectra using HCD at NCE=25 (a). The structure of lAI is shown in (b).

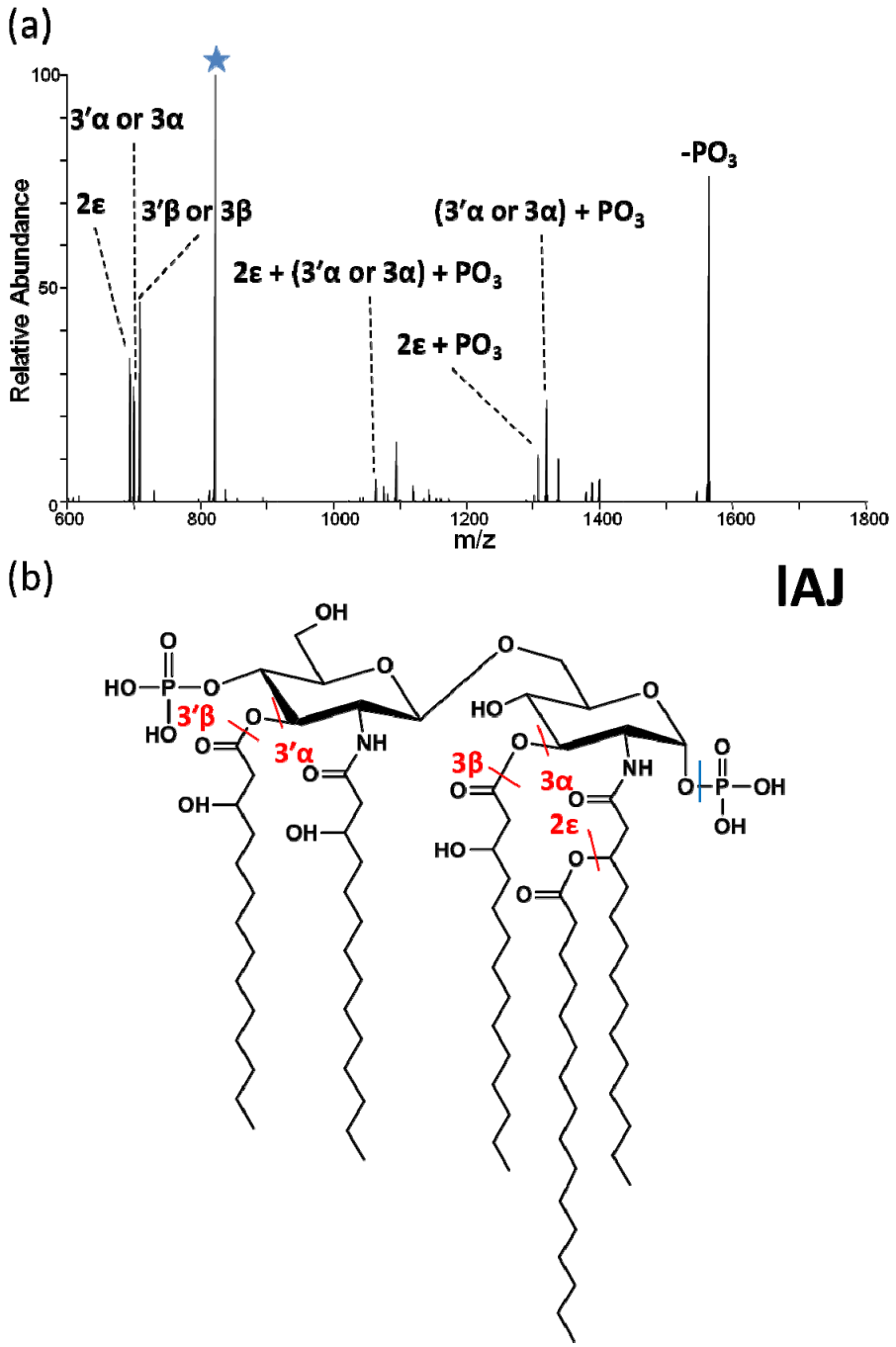

Supplementary Figure S12: lAJ MS2 spectra using HCD at NCE=25 (a). The structure of lAJ is shown in (b).

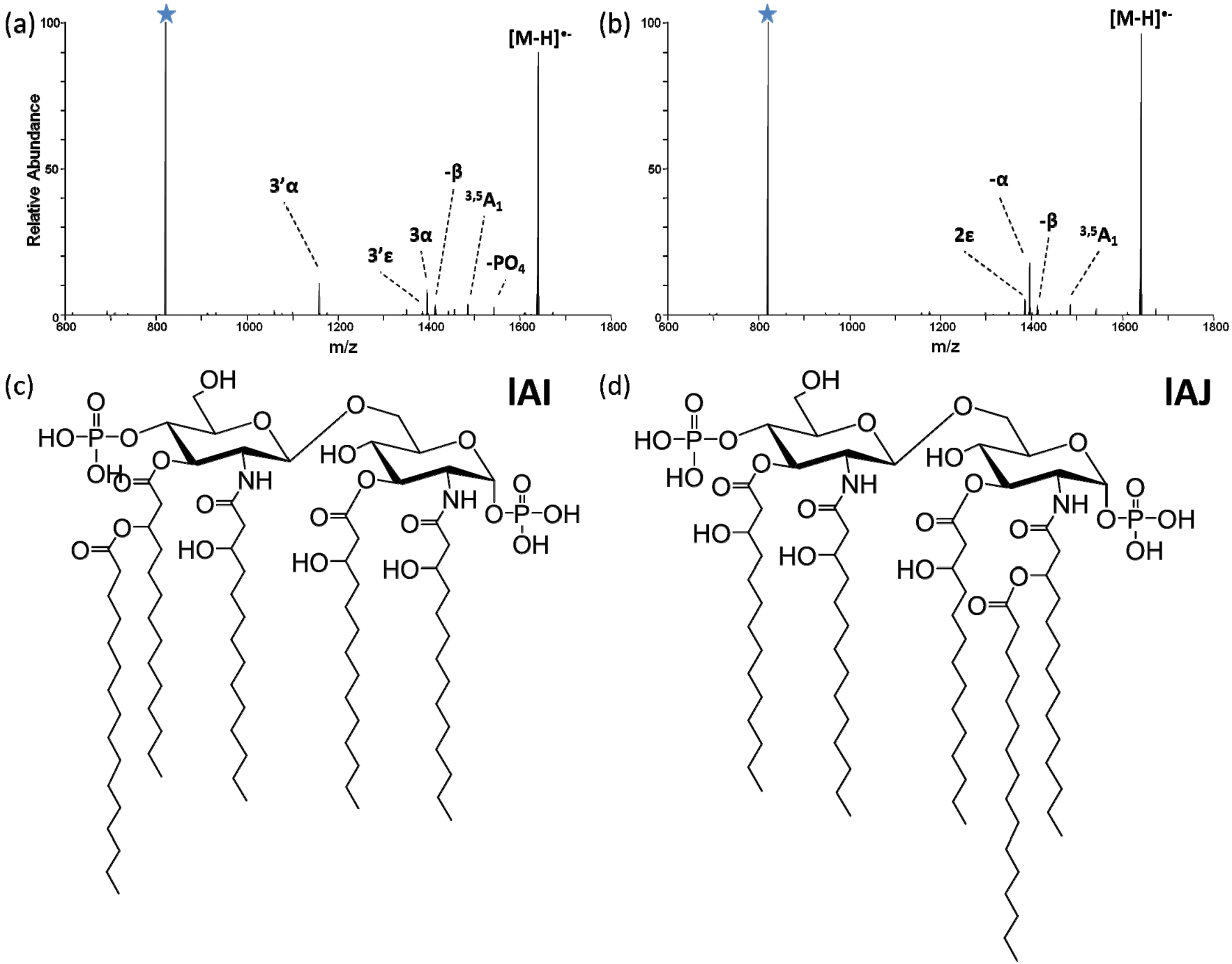

Supplementary Figure 13: MS2 UVPD spectra of (a) lAI and (b) lAJ at 3mJ and 7 pulses and their structures (c) and (d), respectively.

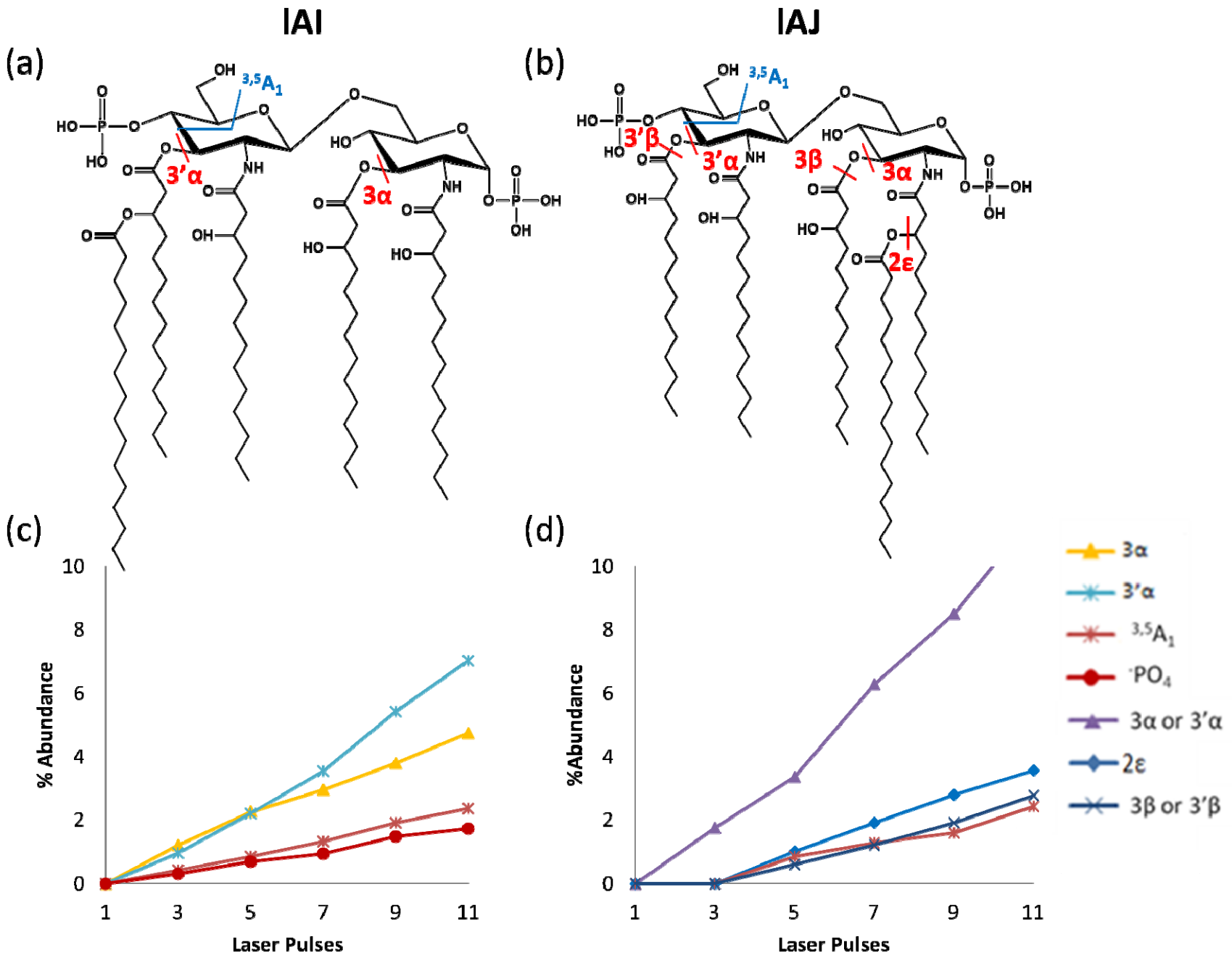

Supplementary Figure 14: Structures of lipid A isomers (a) lAI and (b) lAJ. The UVPD ERMS plots are shown for each doubly deprotonated lipid in (c) and (d), respectively, showing the preference for loss of α-chains over ε-chains.